GSA Data Repository 2016022

An extensive subglacial lake and canyon system in Princess Elizabeth Land, East Antarctica

Stewart S.R. Jamieson[1,*], Neil Ross[2], Jamin S. Greenbaum[3], Duncan A. Young[3], Alan R.A. Aitken[4], Jason L. Roberts[5,6], Donald D. Blankenship[3], Sun Bo[7] and Martin J. Siegert[8]

[1]*Department of Geography, Durham University, South Road, Durham, DH1 3LE, UK*

[2]*School of Geography, Politics and Sociology, Newcastle University, Claremont Road, Newcastle Upon Tyne, NE1 7RU, UK*

[3]*University of Texas Institute of Geophysics, University of Texas at Austin, Austin, Texas 78758, USA*

[4]*School of Earth and Environment, University of Western Australia, Perth, Western Australia 6009, Australia*

[5]*Australian Antarctic Division, Kingston, Tasmania 7050, Australia*

[6]*Antarctic Climate & Ecosystems Cooperative Research Centre, University of Tasmania, Hobart, Tasmania 7001, Australia*

[7]*Polar Research Institute of China, Jinqiao Road, Shanghai 200136, People's Republic of China.*

[8]*Grantham Institute and Department of Earth Science and Engineering, Imperial College London, South Kensington, London, SW7 2AZ, UK*

*E-mail: Stewart.Jamieson@durham.ac.uk

The supplemental information provided here adds detail to the methodology involved in mapping the subglacial channel and lake system, as well as in the derivation and analysis of subglacial and subaerial drainage pathways. In addition, supplemental figures support the work presented in the main manuscript.

MAPPING

The RADARSAT ice surface mosaic (Jezek et al., 2002) records the backscatter of the radar signal across the ice-sheet surface and near-surface (Fig. DR1). Although backscatter can be controlled by a range of factors, it is dominated by changes in the shape of the ice surface. The generation of surface undulations is often controlled by interaction of the ice flow and valleys and ridges beneath the ice (Gudmundsson, 2003). In many parts of Antarctica therefore, the RADARSAT data contain an indirect record of subglacial topography. Similarly, variation in the optical MODIS dataset (Haran et al., 2014; Scambos et al., 2007) reflects variation in ice and snow characteristics as ice flows over topographic features or as snow accumulates or ablates in relation to small ice surface undulations (Fig. DR1). The ice-

surface DEM, which is derived from satellite altimetry (Bamber et al., 2009; Griggs and Bamber, 2009) directly records these minor surface undulations (Fig. DR1). Furthermore, enhanced wind erosion on the crests and snow deposition in the hollows results in the associated surface features having a distinct reflectivity character (Welch and Jacobel, 2005). The topographic influence on ice-surface morphology becomes muted under thicker ice as a consequence of viscous ice deformation. Nevertheless, as shown in previous work (Cianfarra and Salvini, 2014; Golynsky and Golynsky, 2007; Rémy and Minster, 1997; Rose et al., 2014; Ross et al., 2014), by analysing contrasts in satellite ice surface datasets, patterns can be detected that reflect subglacial topographic features.

DRAINAGE ANALYSIS

In order to compare how the presence of the canyons would change subglacial drainage patterns, we compare a series of hydraulic potential drainage systems (Fig. 3). First, we calculate drainage beneath the ice sheet using Bedmap2 data (Fig. 3a). We then do this in a 'canyonised' version of the landscape whilst retaining the modern Bedmap2 ice surface (Fig. 3b). Finally, following Jamieson et al., (2014), we calculate fluvial drainage over an ice-free topography where the landscape has been isostatically rebounded to account for the removal of the modern ice load and for the associated changes in water loading that this would incur (Fig. 3c).

Following Shreve, (1972) we calculate hydraulic potential (ϕ) is a function of bed elevation (h), acceleration due to gravity (g), the density of water (ρ_w) and water pressure (P_w) thus :

$$\phi = \rho_i g h + P_w \qquad (1)$$

where ρ_w and ρ_i are the density of water and ice respectively (1000 kg/m^3 vs. 917 kg/m^3). Water pressure is a function of ice overburden ($\rho_w g H$), where H is the ice thickness, and of effective pressure (N) thus:

$$P_w = \rho_w g H - N \qquad (2)$$

In order to delineate regional-scale drainage, and in the absence of direct measurements of effective pressure, water pressure is assumed to be equal to ice overburden pressure meaning that N=0. As a consequence, hydraulic potential is calculated as:

$$\phi = \rho_i g h + \rho_w g H \qquad (3)$$

Following the calculation of hydraulic potential, internally draining sinks were filled to generate a freely draining system. In all cases, drainage routing follows the path of steepest gradient in the hydraulic potential surface.

For calculations of drainage where the ice has been removed, the drainage follows the steepest slope and internally draining sinks were again filled as in the hydraulic potential drainage calculations.

Figure 3 shows the catchment boundaries that correspond to the different hydraulic conditions in our sensitivity analysis, providing an illustration of the area of the bed which will drain through each system.

CANYONISATION OF TOPOGRAPHY

Across PEL the Bedmap2 bed DEM is based on few absolute measurements (Fig. 1). Therefore, to test whether a topography characterised by canyons would have a significant impact upon subglacial drainage patterns we introduce a 500 m deep, 5 km wide, v-shaped canyon into the Bedmap2 bed dataset along the hypothesised route of our channel system. These canyons are as small as possible based on the 1 km resolution of Bedmap2 and have sidewall slopes of 10°, shallower than the canyon identified by RES data in Figure 2 and conservative in comparison to the depth and likely sidewall angles of recently identified subglacial canyons in Greenland (Bamber et al., 2013). The hypothesised subglacial lake is also added into the Bedmap2 DEM and deepens conservatively and linearly to 500 m depth along its central-axis. The lakes side slopes are shallower than the canyons because the 500 m depth of the lake tapers to 0 m depth at the margin of the lake as opposed to at a set number of cells distance from the lake center.

MELTWATER OUTFLOW AT THE GROUNDING LINE

Assuming that the bed is at the pressure melting point, the canyon and lake system is likely to function as an interconnected subglacial drainage network that extends across the centre of PEL. This is confirmed by an ICECAP radar profile acquired only a few km inland of the grounding line which contains two deep subglacial canyons running perpendicular to the coast (Channels A and B in Figs. DR3a and DR3b).

A second, parallel ICECAP RES profile which crosses the West Ice Shelf, suggests current or very recent drainage of subglacial water across the grounding line via canyons A and B (Figs. DR3a and DR3b). For example, in the area immediately beyond the grounding line adjacent to channel A, the base and surface of the ice shelf is very smooth in contrast to the heavily-

crevassed ice shelf surface and rough ice-ocean interface on either side (Fig. DR3c). In addition, a significant undulation in the ice shelf base that measures ca. 20 km wide and ca. 200 m high, and is characterised by a smooth ice-water interface is present directly down stream of channel A (Fig. DR3). It is possible that this ice shelf feature may be a result of focussed delivery of subglacial water to the grounding line, leading to locally enhanced ice shelf basal melt (Le Brocq et al., 2013). In accordance with hydrostatic equilibrium, a depression in the ice shelf surface coincides with the basal feature. Downstream of the second, deeper, channel (B) beneath the grounded ice (Fig. DR3b), a pair of narrow ca. 120 m relief channels are visible in the base of the ice shelf. These could also be the result of localised melting beneath the ice shelf caused by focussed subglacial water discharge (Le Brocq et al., 2013) but which has diverged either side of Mikhaylov Island (Fig. DR3c). An alternative explanation for the presence of the channels and smooth undulations in the base of the ice shelf is that warm ocean water is melting the underside of the shelf in very localised areas. We note however, that there is remarkable coincidence between the location of the canyons as they cross the grounding line, and the locations of these features in the ice shelf base.

SUPPLEMENTAL FIGURES

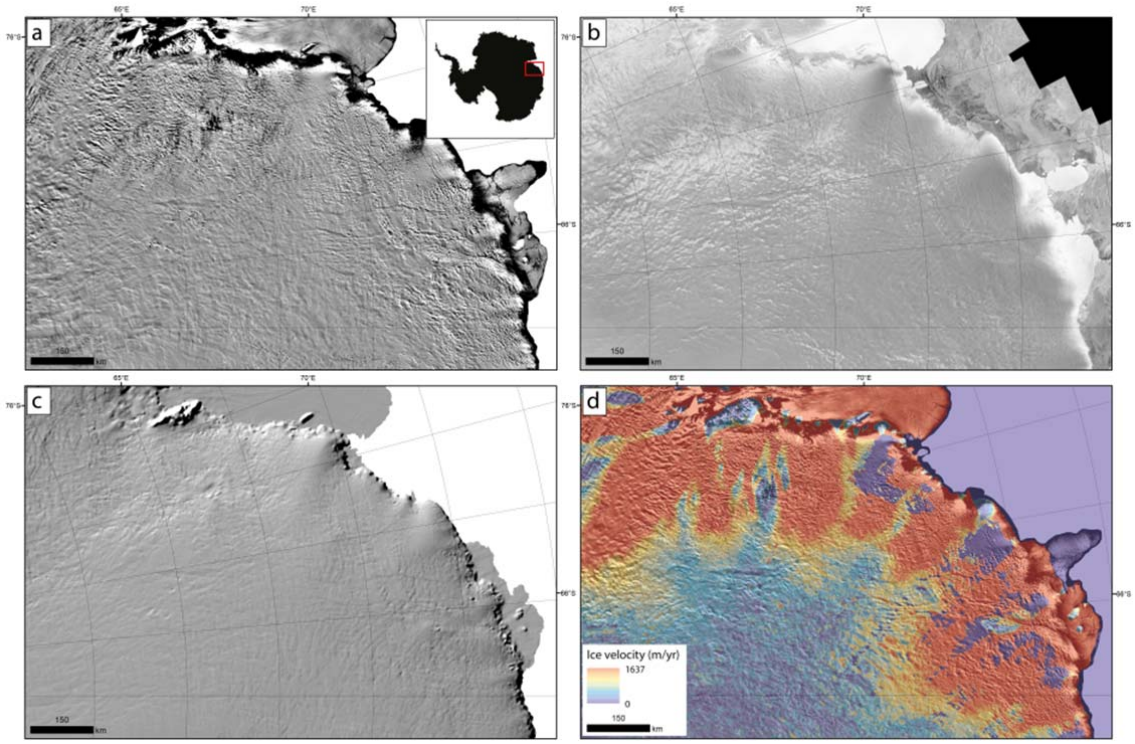

Figure DR1: Key ice surface datasets over PEL. a: MODIS MOA 2009 (Haran et al., 2014; Scambos et al., 2007); b: RADARSAT (Jezek et al., 2002); c: Hillshade of the ice surface

DEM (Bamber et al., 2009; Griggs and Bamber, 2009); d: MeaSUREs ice surface velocity underlain by MOA data (Rignot et al., 2011).

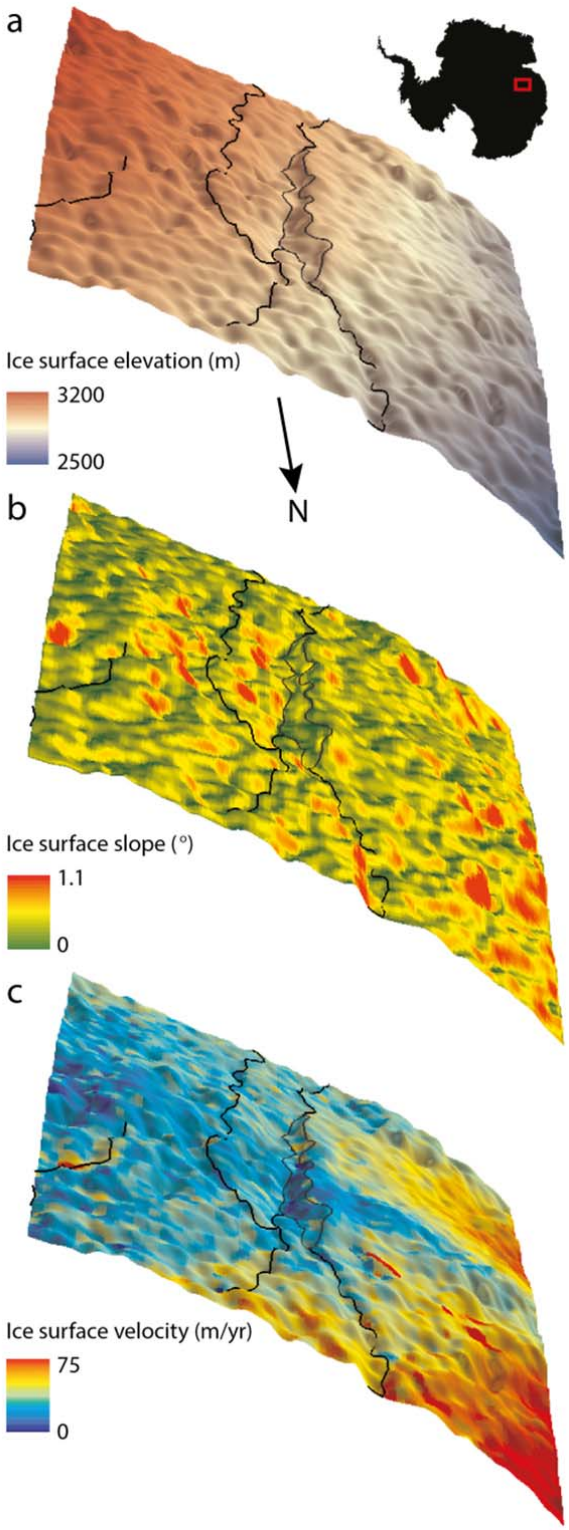

Figure DR2: 3D perspectives of the ice surface characteristics surrounding the hypothesised lake area and canyons (black lines) showing ice surface elevation (a), ice surface slope (b) and ice surface velocity (c).

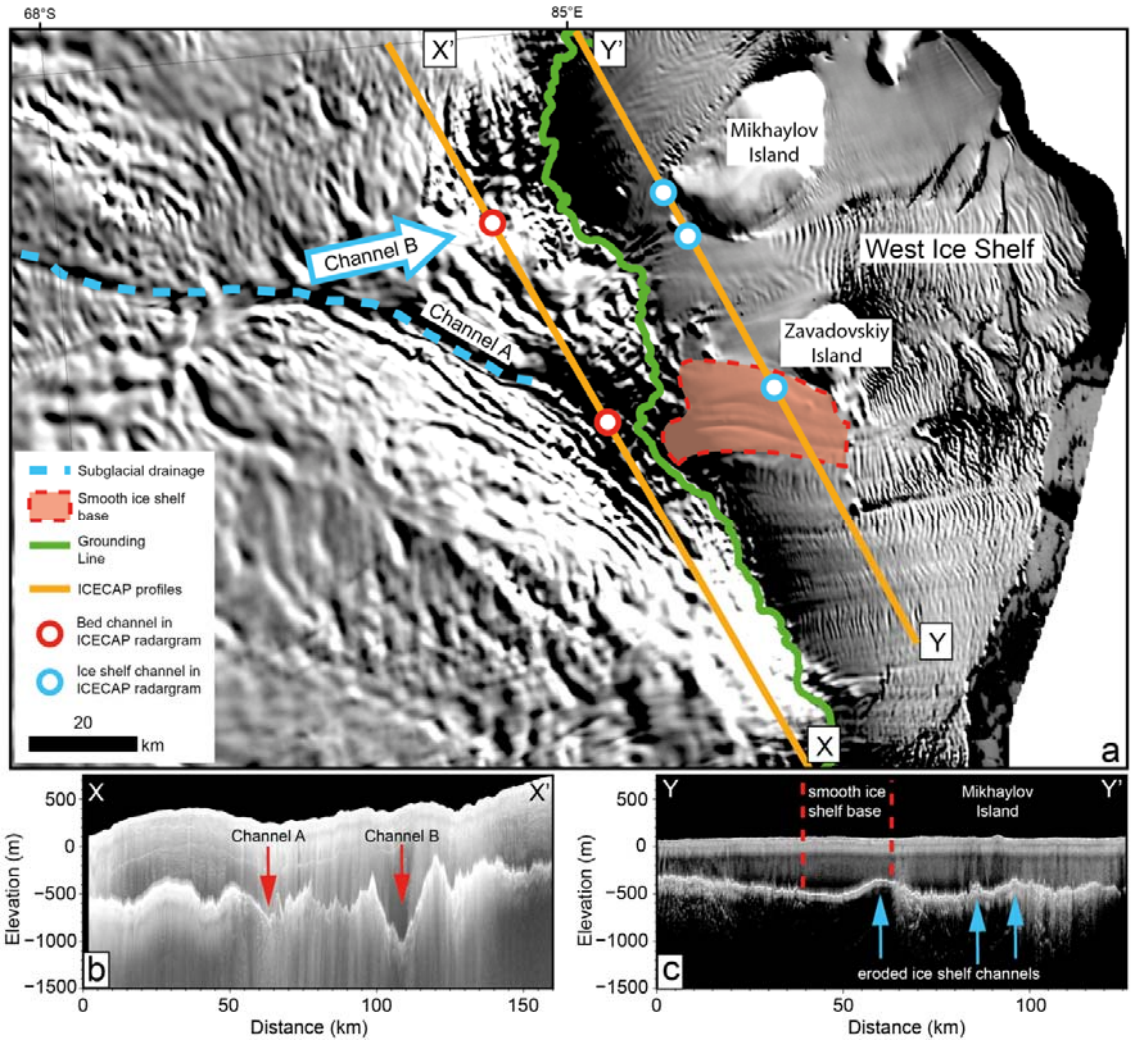

Figure DR3: The coastal terminus of a mapped subglacial channel as it meets the West Ice Shelf (see Fig. 1 for location). a) At the grounding line, water drained from PEL is discharged into the ocean and may smooth the underside of the floating ice. The blue arrow shows a possible drainage pathway based on data in panel b not mapped from ice surface analysis. Orange lines are ICECAP RES profiles where, following data in panels b and c, red dots indicate bedrock channel locations and blue dots correspond to channels in the underside of the ice shelf. b) the subglacial topography immediately inland of the grounding line contains at least 2 subglacial channels (red arrows) which align with channels mapped from ice surface data. X-X' lies on ICECAP line PEL/JKB2h/Y16a. c) the morphology of the ice shelf base in the area beyond where the channels discharge across the grounding line. The ice shelf base has some smoothing (between red dashed lines) and contains at least 3 channels in its base (blue arrows), all of which align with the bedrock channels on the terrestrial margin. Profile Y-Y' lies on ICECAP line PEL/JKB2h/Y13b.

REFERENCES CITED

Bamber, J. L., Gomez-Dans, J. L., and Griggs, J. A., 2009, A new 1 km digital elevation model of the Antarctic derived from combined satellite radar and laser data – Part 1: Data and methods: The Cryosphere, v. 3, no. 1, p. 101-111.

Bamber, J. L., Siegert, M. J., Griggs, J. A., Marshall, S. J., and Spada, G., 2013, Paleofluvial Mega-Canyon Beneath the Central Greenland Ice Sheet: Science, v. 341, no. 6149, p. 997-999.

Cianfarra, P., and Salvini, F., 2014, Ice sheet surface lineaments as nonconventional indicators of East Antarctica bedrock tectonics: Geosphere, v. 10, no. 6, p. 1411-1418.

Golynsky, D. A., and Golynsky, A. V., 2007, Gaussberg rift - illusion or reality?, *in* Cooper, A. K., and Raymond, C. R., eds., Antarctica: A Keystone in a Changing World: Online Proceedings of the 10th International Symposium of AntarcticEarth Science, Volume Open-File Report 2007-1047, Extended Abstract 168, USGS, p. 5.

Griggs, J. A., and Bamber, J. L., 2009, A New 1 km Digital Elevation Model of Antarctica Derived from Combined Radar and Laser Data Part 2: Validation and Error Estimates. : The Cryosphere, v. 3, p. 113-123.

Gudmundsson, H., 2003, Transmission of basal variability to a glacier surface: Journal of Geophysical Research, v. 108, no. B5.

Haran, T. M., Bohlander, J., Scambos, T., Painter, T. H., and Fahnestock, M., 2014, MODIS Mosaic of Antarctica 2008-2009 (MOA2009) Image Map. Subset hp1.: Boulder, Colorado USA: National Snow and Ice Data Center.

Jezek, K., Curlander, J. C., Carsey, F., Wales, C., and Barry, R., 2002, RAMP AMM-1 SAR Image Mosaic of Antarctica. Version 2: National Snow and Ice Data Center, Boulder, CO.

Le Brocq, A. M., Ross, N., Griggs, J. A., Bingham, R. G., Corr, H. F. J., Ferraccioli, F., Jenkins, A., Jordan, T. A., Payne, A. J., Rippin, D. M., and Siegert, M. J., 2013, Evidence from ice shelves for channelized meltwater flow beneath the Antarctic Ice Sheet: Nature Geosci, v. 6, no. 11, p. 945-948.

Rémy, F., and Minster, J.-F., 1997, Antarctica Ice Sheet Curvature and its relation with ice flow and boundary conditions: Geophysical Research Letters, v. 24, no. 9, p. 1039-1042.

Rignot, E., Mouginot, J., and Scheuchl, B., 2011, Ice Flow of the Antarctic Ice Sheet: Science, v. 333, no. 6048, p. 1427-1430.

Rose, K. C., Ross, N., Bingham, R. G., Corr, H. F. J., Ferraccioli, F., Jordan, T., Le Brocq, A. M., Rippin, D. M., and Siegert, M. J., 2014, A temperate former West Antarctic ice sheet suggested by an extensive zone of subglacial meltwater channels: Geology.

Ross, N., Jordan, T. A., Bingham, R. G., Corr, H. F. J., Ferraccioli, F., Le Brocq, A. M., Rippin, D. M., Wright, A. P., and Siegert, M. J., 2014, The Ellsworth Subglacial Highlands: Inception and retreat of the West Antarctic Ice Sheet: Geological Society of America Bulletin, v. 126, no. 1-2, p. 3-15.

Scambos, T. A., Haran, T. M., Fahnestock, M. A., Painter, T. H., and Bohlander, J., 2007, MODIS-based Mosaic of Antarctica (MOA) data sets: Continent-wide surface morphology and snow grain size: Remote Sensing of Environment, v. 111, no. 2–3, p. 242-257.

Shreve, R. L., 1972, Movement of water in glaciers: Journal of Glaciology, v. 11, p. 205-214.

Welch, B. C., and Jacobel, R. W., 2005, Bedrock topography and wind erosion sites in East Antarctica: observations from the 2002 US-ITASE traverse: Annals of Glaciology, v. 36, no. 122, p. 3-10.